

Universality in edge-source diffusion dynamics

Niels Asger Mortensen, Fridolin Ockels, and Henrik Bruus

MICRO Department of Micro and Nanotechnology, NanoDTU,
Technical University of Denmark, Bldg. 345 east, DK-2800 Kgs. Lyngby, Denmark.
(Dated: December 9, 2005)

We show that in edge-source diffusion dynamics the integrated concentration $N(t)$ has a universal dependence with a characteristic time-scale $\tau = (A/P)^2 = (4D)^{-1}$, where D is the diffusion constant while A and P are the cross-sectional area and perimeter of the domain, respectively. For the short-time dynamics we find a universal square-root asymptotic dependence $N(t) = N_0 \sqrt{t}$ while in the long-time dynamics $N(t)$ saturates exponentially at N_0 . The exponential saturation is a general feature while the associated coefficients are weakly geometry dependent.

PACS numbers: 02.40.-k, 66.10.Cb, 87.15.Vv

Concepts like diffusion and Brownian motion are central in a wide range of complex dynamical phenomena [1, 2] including diffusion of ions through biological membranes, neutron diffusion in nuclear reactors, charge-carrier diffusion in semiconductors, diffusion of heat in any substance, diffusion of momentum in fluids, and diffusion of photons in the interior of the Sun [3, 4, 5, 6]. In its simplest form of a scalar quantity c the diffusion dynamics is governed by the linear partial differential equation

$$D \nabla^2 c(\mathbf{r}; t) = \partial_t c(\mathbf{r}; t); \quad (1)$$

where D is the diffusion constant. With the above notation we have emphasized diffusion of matter (with concentration c), but we note that the same equation also governs diffusion of energy such as in thermal problems where Eq. (1) is often referred to as the heat equation. Despite its apparent simplicity the link between space and time variables \mathbf{r} and t typically makes diffusion dynamics strongly dependent on the geometry and initial conditions. In this paper we find an exception to this and report a universality in edge-source diffusion dynamics. Assuming perfect translation invariance along the z di-

rection, we consider a cross section Ω in the xy plane, see Fig. 1, where chemical species or heat is supplied at the boundary $\partial\Omega$. For simplicity we imagine a situation with a constant concentration c_0 outside while the domain itself is empty, $c(\mathbf{r}; t < 0) = 0$ for $\mathbf{r} \in \Omega$, before the onset of diffusion at $t = 0$.

Recently, pressure-driven flow in steady-state was analyzed in the framework of simple geometrical measures [7] such as the cross-sectional area $A = \int_{\Omega} d\mathbf{r}$, the perimeter of the boundary $P = \int_{\partial\Omega} d\ell$, and the compactness $C = P^2/A$. In the following we study the importance of these parameters for diffusion dynamics and in particular for the integrated concentration $N(t)$ given by

$$N(t) = \int_{\Omega} c(\mathbf{r}; t); \quad (2)$$

with the limits $N(t \rightarrow 0) = 0$ and $N(t \rightarrow \infty) = c_0 A$ implied by the boundary and initial conditions for c .

Dimensional analysis. As a first step in solving the dynamics of the integrated concentration $N(t)$ one might estimate the time-scale for filling up the domain. Obviously, increasing the area A results in an increasing

filling time, while increasing the perimeter P or the diffusion constant D results in a decreasing filling time. By dimensional analysis we thus arrive at $\tau = (A/P^2)^{-1} = D^{-1}$ which, as we shall see, is indeed a good estimate since detailed analysis yields

$$\tau = \frac{A}{P^2} \frac{1}{4D}; \quad (3)$$

Short-time diffusion dynamics. On a short time-scale the diffusion is perpendicular to the boundary and thus the problem is quasi-one dimensional. By a short time-scale we here mean $\tau \ll L_{\partial}^2/D$ where L_{∂} is a characteristic length scale (such as the local radius of curvature) for shape variations along the boundary $\partial\Omega$. We base our analysis on the well-known method of combination of variables originally introduced by Boltzmann [5, 8]: normalization of length scales by $\sqrt{4Dt}$ reduces Eq. (1)

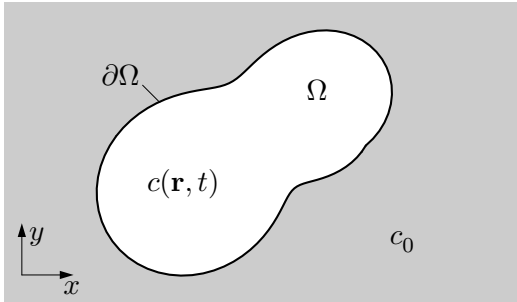


FIG. 1: A sketch of the cross section Ω (white) with boundary $\partial\Omega$ (black curve) in the xy -plane of a rod with translational invariance in the z direction. At time $t = 0$, where the concentration $c(\mathbf{r}; t)$ inside Ω is zero, diffusion is suddenly turned on from the outside, where the concentration is kept at the constant value c_0 (gray).

TABLE I: The parameters λ_1 Eq. (9) and λ_2 Eq. (11) for the lowest eigenfunction for differently shaped cross sections.

Cross section	λ_1	λ_2
Circle	$\frac{2}{16} \sqrt{\frac{1}{16}} = 1.14$	$4 = \frac{2}{0.1} = 0.69$
Half-circle	$\frac{2}{(4 + 8\pi)^2} \sqrt{\frac{1}{16}} = 1.08$	0.64^a
Quarter-circle	$\frac{2}{(4 + 16\pi)^2} \sqrt{\frac{1}{16}} = 1.00$	0.65^a
Ellipse (1:2)	1.18^a	0.67^a
Ellipse (1:3)	1.21^a	0.62^a
Ellipse (1:4)	1.23^a	0.58^a
Triangle (1:1:1) ^b	$\frac{3}{16} = 0.86$	$6 = \frac{2}{0.1} = 0.61$
Triangle (1:1:2) ^c	$\frac{5}{16(2 + \sqrt{2})^2} = 0.83$	$512 = 9 = \frac{2}{0.1} = 0.58$
Square (1:1)	$\frac{3}{16} = 0.97$	$64 = \frac{4}{0.1} = 0.66$
Rectangle (1:2)	$\frac{5}{16} = 1.44 = 1.08$	$64 = \frac{4}{0.1} = 0.66$
Rectangle (1:3)	$\frac{5}{16} = 1.28 = 1.21$	$64 = \frac{4}{0.1} = 0.66$
Rectangle (1:4)	$\frac{17}{16} = 4.00 = 1.32$	$64 = \frac{4}{0.1} = 0.66$
Rectangle (1:1)	$\frac{3}{16} = 1.6 = 1.94$	$64 = \frac{4}{0.1} = 0.66$
Rectangle (w:h)	$\frac{3}{16} \frac{C}{C} = 8; C = \frac{4(h+w)^2}{hw}$	$64 = \frac{4}{0.1} = 0.66$
Pentagon	1.02^a	0.67^a
Hexagon	1.05^a	0.68^a

^aData obtained by finite-element simulations [10].

^bSee e.g. Ref. 11 for the eigenfunctions and eigenspectrum.

^cSee e.g. Ref. 12 for the eigenfunctions and eigenspectrum.

to a 1D ordinary differential equation with the solution

$$\frac{c(r;t)}{c_0} = \text{erfc} \left(\frac{d_2(r)}{\sqrt{4Dt}} \right); \quad (4)$$

where $d_2(r)$ is the normal distance to the boundary and $\text{erfc}(x)$ is the complementary error function. For t the integrated concentration $N(t)$ becomes

$$N(t) = P \int_0^{\lambda_1} ds c_0 \text{erfc} \left(\frac{s}{\sqrt{4Dt}} \right) = N_0 \frac{\lambda_1}{\sqrt{4Dt}}; \quad (5)$$

where we have introduced the characteristic time scale defined in Eq. (3) and $N_0 = c_0 A$. The square-root dependence is a universal property for geometries with sufficiently smooth boundaries and dynamics deviating from this dependence is referred to as anomalous. Previous work on the heat content in the crushed ice model has reached results equivalent to Eq. (5) for the heat contents [9].

Long-time diffusion dynamics. Since $N(t) \rightarrow N_0$ the result in Eq. (5) is of course only meaningful for $t \rightarrow \infty$.

When time becomes comparable to τ a saturation will occur due to decreasing gradients in density. For structures without high symmetries the saturation will be accompanied by an onset of diffusion parallel to the boundary ∂ , and in this limit the dynamics will be slow compared to the initial behavior, Eq. (5). To study this we first derive a continuity equation by applying Green's

theorem to Eq. (1),

$$\frac{d}{dt} \int_{\partial} d\mathbf{n} \cdot \mathbf{r} c(r;t) = - \int_{\partial} d\mathbf{n} \cdot \mathbf{r} \nabla c(r;t); \quad (6)$$

Here, \mathbf{n} is a normal vector to ∂ , the integral is a line integral along ∂ , and $\mathbf{r} \cdot \nabla c$ is naturally interpreted as a current density. Next, we note that for long time-scales we have to a good approximation that $\mathbf{n} \cdot \mathbf{r} c(r;t) / c_0 = N(t) / A$ is constant along the boundary so that

$$N_0 = N(t) / A; \quad (7)$$

resulting in an exponentially decaying difference. This may also be derived from an eigenfunction expansion,

$$\frac{c(r;t)}{c_0} = 1 - \sum_n f_n(r) e^{-\lambda_n^2 t}; \quad (8)$$

which upon substitution into the diffusion equation yields a Helmholtz eigenvalue problem for λ_n and f_n ,

$$\nabla^2 f_n(r) = -\lambda_n^2 f_n(r); \quad (9)$$

with $f_n(r) = 0$ for $r \in \partial$. Eq. (8) and the initial condition $c(r;t=0) = c_0$ imply that $\sum_n f_n(r) = 1$ and thus $f_n = \frac{1}{A} \frac{d}{dr} \left(\frac{r}{\lambda_n} \right) = \frac{1}{A} \frac{d}{dr} \left(\frac{r}{\lambda_n} \right)$. The long-time dynamics is governed by the lowest eigenvalue λ_1 yielding

$$\frac{N(t)}{N_0} = 1 - \sum_n f_n \exp \left(-\lambda_n^2 t \right) \approx 1 - \lambda_1^2 \frac{t}{A}; \quad (10)$$

where

$$\lambda_n = \frac{A_n}{A}; \quad A_n = \frac{1}{A} \frac{d}{dr} \left(\frac{r}{\lambda_n} \right)^2; \quad (11)$$

As often done in optics [13], A_n can be interpreted as the effective area covered by the n th eigenfunction. Values for a selection of geometries are tabulated in Table 1. The circle is the most compact shape and consequently it has the largest value for λ_1 , or put differently the mode has the relatively largest spatial occupation of the total area. The normalized eigenvalue λ_1 is of the order unity for compact shapes and in general it tends to increase slightly with increasing surface to area ratio $P = A$. The modest variation in both λ_1 and λ_2 among the various geometries suggests that the overall dynamics of $N(t)$ will appear almost universal and that, e.g., Eq. (10) for the circle (mathematical details follow below),

$$\frac{N(t)}{N_0} = 1 - \frac{4}{\pi} \exp \left(-\frac{t}{16} \right); \quad \lambda_1 = 0.1; \quad \lambda_2 = 5.783; \quad (12)$$

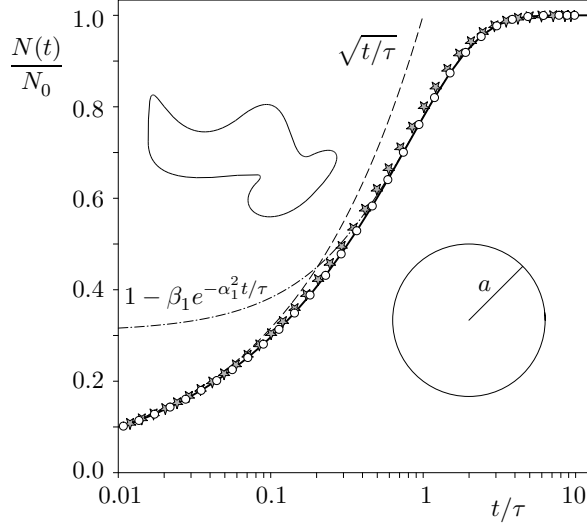


FIG. 2: A lin-log plot of $N(t)/N_0$ as a function of t/τ for a circular cross section (white circles) and for an arbitrarily shaped cross section (gray stars); both shapes are shown in the insets. The solid line shows the exact result for the circle, i.e., the first 1000 terms in the infinite series Eq. (14), the dashed line shows the short-time asymptotic expression Eq. (5), the dot-dashed line shows the long-time asymptotic expression Eq. (12) for the circle with $\alpha_{0,1} = \alpha_{0,1}^2 = 16$ and $\beta_1 = 4 = \frac{2}{\alpha_{0,1}^2}$, while the data-points are the results of time-dependent finite-element simulations.

will account quantitatively well even for highly non-circular cross sections.

Analytical and numerical examples. In the following we consider a number of geometries and compare the above asymptotic expressions to analytical and numerical results. For the numerics we employ time-dependent finite-element simulations [10] and solve Eq. (1) with a subsequent numerical evaluation of the integrated concentration, Eq. (2).

The circular cross section serves as a reference and an illustrative example where we directly can compare the above limits to analytical and numerical results. Applying the method of separation of variables yields [5]

$$\frac{c_{\text{circ}}(r;t)}{c_0} = 1 - \sum_{n=1}^{\infty} \frac{J_0(\alpha_{0,n} r/a)}{J_1(\alpha_{0,n})} e^{-\frac{\alpha_{0,n}^2 D t}{a^2}}; \quad (13)$$

where a is the radius and $\alpha_{0,n}$ is the n th zero of the m th Bessel function of the first kind, $J_m(\alpha_{0,n}) = 0$. By a straightforward integration over the cross section we get

$$\frac{N_{\text{circ}}(t)}{N_0} = 1 - \sum_{n=1}^{\infty} \frac{4}{\alpha_{0,n}^2} \exp\left(-\frac{\alpha_{0,n}^2 D t}{16 a^2}\right); \quad (14)$$

where we have made the time-scale explicit, see Eq. (3). This result can also be derived using the continuity equation, Eq. (6). For $t > \tau$ the series converges rapidly, and keeping only the first term we arrive at Eq. (12).

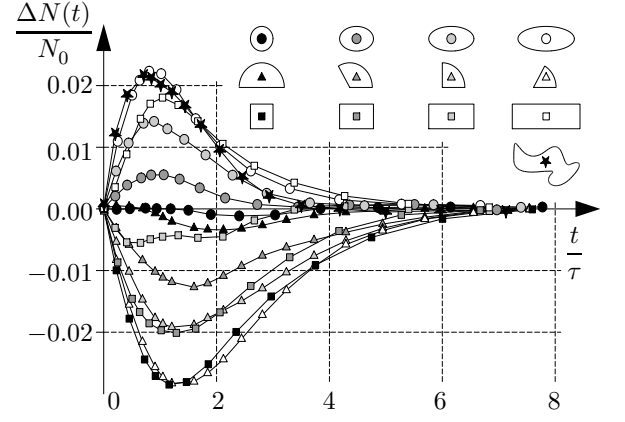


FIG. 3: Plot of the deviation $N(t) - N_0$ from the circular case, Eq. (15), as a function of t/τ for different cross sections (see insets). The data-points are results of finite-element simulations. The ellipses have eccentricities 1;1.5;2 and 2.5, the circle sectors have angles $\pi/2$; $\pi/3$; $\pi/2$ and $\pi/3$, and the rectangles have aspect ratios 1;1.5;2 and 3. Note how the maximal deviation is less than 0.03 or 3%.

In Fig. 2 we compare the asymptotic results, Eqs. (5) and (12) with the exact result, Eq. (14), as well as with time-dependent finite-element simulations. As seen both the short-time square-root and long-time exponential dependencies are in good agreement with the exact results as well as with the simulations. Fig. 2 also includes numerical results for an arbitrarily shaped cross section and, as suggested above, we see that Eqs. (5) and (12) account remarkably well even for this highly non-circular shape.

In order to see how well Eq. (14) accounts for other non-circular geometries we have employed time-dependent finite-element simulations to numerically study the relative deviations $N - N_0$ from it,

$$\frac{N(t) - N_0}{N_0} = \frac{N(t) - N_{\text{circ}}(t)}{N_0}; \quad (15)$$

Figure 3 summarizes results for a number of geometries. In all cases the dynamics at small times $t < \tau$ is in full accordance with the predicted square-root dependence, Eq. (5), and for long times the predicted exponential dependence, Eq. (12), fits the dynamics excellently. For the dynamics around $t \approx \tau$ deviations from the circular result are well within 3% for the considered highly non-circular geometries.

Discussion and conclusion. We have shown that edge-source diffusion dynamics in a rod of arbitrary cross section has an intrinsic time-scale $\tau = (A/P)^2/(4D)$, with D being the diffusion constant while A and P are the cross-sectional area and perimeter of Ω , respectively. Initially, the scaling $N(t) \propto \sqrt{t}$ follows a universal square-root dependence $N(t) = N_0 \sqrt{t/\tau}$, irrespectively of the shape of the domain Ω . For longer times $N(t)$ saturates exponentially at N_0 . The saturation is governed by the lowest dimensionless eigenvalue $\alpha_{0,1}$ of the Helmholtz equation

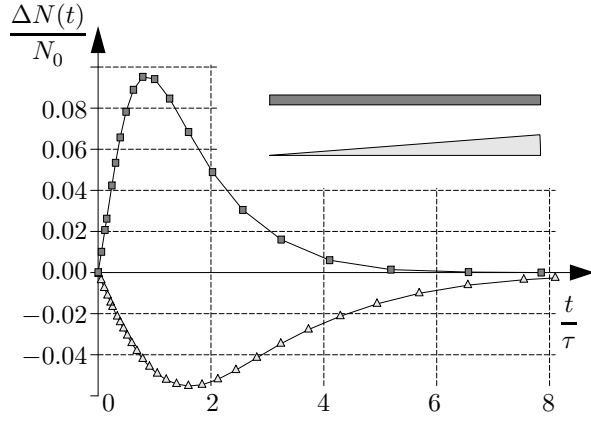


FIG. 4: Plots as in Fig. 3 but here for two extreme geometries: a sector of a circular disc with angle $2\arctan(l=30)$ and a rectangle with aspect ratio $l=30$, see insets. While these two shapes have nearly the same area and perimeter, the former diffuses slower than the circular cross section and the latter faster. The maximal deviations are -6% and $+10\%$, respectively.

rather than the full spectrum. Since λ_1 depends only weakly on the geometry the dynamics becomes almost universal. Numerically, we have observed that the deviation from strict universality is typically less than a few percent.

The diffusion problem presented here relates to the question posed by Mark Kac [14]: "Can one hear the shape of a drum?". In the present diffusion problem knowledge about the short-time dynamics allows one to extract the area to perimeter ratio $A=P$ while the shape itself cannot be inferred. For the long-time diffusion dynamics strict universality would require that different shapes have Helmholtz eigenfunctions with the same set of eigenvalues λ_n (isospectrality) and effective areas A_n . However, since the answer to the question of Kac in most cases is positive, see however Refs. [15, 16], the eigenfunction properties λ_n and A_n of different geometries differ. It is thus only the short-time dynamics which is strictly universal while, as mentioned above, the long-time dynamics depends weakly on shape through the first dimensionless eigenvalue λ_1 and the corresponding dimensionless effective area A_1 .

Our simulations support these conclusions, see Fig. 3, and even for extreme shapes such as the narrow disc sector with angle $2\arctan(l=30)$ and the flat rectangle with aspect ratio $l=30$ the deviations from Eq. (14) are less than 10% around $t = \tau$, see Fig. 4. These extreme shapes have almost the same area and perimeter while the eigenfunction properties λ_n and A_n are very different, e.g., λ_1 is constant $64=l^4$ for all rectangles, see Table I, while it scales as l^{-2} for the disc sector with angle $\theta=l$. For any aspect ratio $h=w$ the lowest eigenfunction $\psi_1 = \sin(x/w)\sin(y/h)$ of the rectangle is nearly uniformly distributed in Ω , and the shape favors rapid perpendicular diffusion resulting in a falling slightly faster

than for the circular shape. For the disc sector with angle $\theta=l$ the lowest eigenfunction $\psi_1 = J_m(\lambda_{m,1}r/a)\sin(m\phi)$ is confined to a region of width $a=m^{-1/3}$ near the circular edge. This shortens the effective perimeter resulting in a falling time longer than for the circular shape. It is thus possible to find extreme shapes where $A=P$ is no longer the characteristic length-scale for the long-time diffusion dynamics. The same applies for a cross section with the shape of a tear drop [17], and for more exotic geometries, such as cross sections with a fractal polygonal boundary [18], we expect more severe deviations from the dynamics reported here. However, the deviations from strict universality obtained by extending the short-time scale to the long-time regime are remarkably small.

Apart from the fascinating and intriguing physics involved we believe our results are important to a number of practical problems including mass diffusion in microfluidic channels and heat diffusion in arbitrarily shaped rods.

Acknowledgments. We thank Steen Markvorsen and Ole Hansen for stimulating discussions and Michiel van den Berg for directing our attention to previous work. This work is supported by the Danish Technical Research Council (Grant Nos. 26-03-0073 and 26-03-0037).

-
- [1] P. Hanggi, J. Luczka, and P. Talkner, *New J. Phys.* 7 (2005), Focus on Brownian Motion and Diffusion in the 21st Century.
 - [2] P. Hanggi and F. Marchesonia, *Chaos* 15, 026101 (2005), Introduction: 100 years of Brownian motion.
 - [3] L.D. Landau and E.M. Lifshitz, *Fluid Mechanics*, vol. 6 of Landau and Lifshitz, *Course of Theoretical Physics* (Butterworth (Heinemann, Oxford, 1987), 2nd ed.
 - [4] H. Smith and H.H. Jensen, *Transport Phenomena* (Oxford University Press, Oxford, 1989).
 - [5] E.L. Cussler, *Diffusion mass transfer in fluid systems* (Cambridge University Press, Cambridge, UK, 1997), 2nd ed.
 - [6] R.B. Bird, W.E. Stewart, and E.N. Lightfoot, *Transport Phenomena* (John Wiley & Sons, New York, 2002).
 - [7] N.A. Mortensen, F. Økkel, and H. Bruus, *Phys. Rev. E* 71, 057301 (2005).
 - [8] L. Boltzmann, *Wied. Ann.* 53, 959 (1894).
 - [9] M. van den Berg and J.-F. Le Gall, *Math. Z.* 215, 437 (1994).
 - [10] Comsol/Femlab 3.2, www.comsol.com.
 - [11] M. Brack and R.K. Bhaduri, *Semiclassical Physics* (Addison Wesley, New York, 1997).
 - [12] P.M. Morse and H. Feshbach, *Methods of Theoretical Physics* (McGraw Hill, New York, 1953).
 - [13] N.A. Mortensen, *Opt. Express* 10, 341 (2002).
 - [14] M. Kac, *Am. Math. Mon.* 73, 1 (1966).
 - [15] C. Gordon, D.L. Webb, and S. Wolpert, *Bull. Amer. Math. Soc.* 27, 134 (1992).
 - [16] S. Sridhar and A. Kudrolli, *Phys. Rev. Lett.* 72, 2175 (1994).
 - [17] E. Weisstein, in *MathWorld* (A Wolfram

- Web Resource (Wolfram Research, Inc., 1999),
<http://mathworld.wolfram.com/TeardropCurve.html>
- [18] M. van den Berg and F. den Hollander, Proc. London Math. Soc. 78, 627 (1999).